Journal of Molecular Graphics and Modelling 40 (2013) 99–109

Contents lists available at SciVerse ScienceDirect

Journal of Molecular Graphics and Modelling

journal homepage: www.elsevier.com/locate/JMGM

Mechanism of the irreversible inhibition of human cyclooxygenase-1 by aspirin as predicted by QM/MM calculations

L. Tóth [a], L. Muszbek [a,b], I. Komáromi [b,*]

[a] Clinical Research Center, Medical and Health Science Center, University of Debrecen, Debrecen, Hungary
[b] Vascular Biology, Thrombosis and Haemostasis Research Group of the Hungarian Academy of Sciences at the University of Debrecen, Debrecen, Hungary

ARTICLE INFO

Article history:
Accepted 28 December 2012
Available online 9 January 2013

Keywords:
Cyclooxygenase
Aspirin
Molecular modeling
QM/MM
ONIOM
Reaction mechanism

ABSTRACT

Acetylsalicylic acid (aspirin) suppresses the generation of prostaglandin H2, which is the precursor of thromboxane A2. Aspirin acts as an acetylating agent in which its acetyl group is covalently attached to a serine residue (S530) in the active site of the cyclooxygenase-1 enzyme. The exact reaction mechanism has not been revealed by experimental methods.

In this study the putative structure of human cyclooxygenase-1 was constructed from ovine cyclooxygenase-1 by homology modeling, and the acetylsalicylic acid was docked into the arachidonic acid binding cavity of the enzyme. To characterize the shape of the potential energy surface of the acetylating reaction and to determine the relative energies of the stationary points on the surface, a series of ONIOM-type quantum mechanical/molecular mechanical (QM/MM) calculations were carried out at different QM levels of theories applying electronic embedding approximations. The acetylsalicylic acid and the surrounding amino acids were included in these calculations. Frequency analyses were performed to prove the existence of first order saddle points (representing transition states) and local minima on the potential energy surface.

It was found that all levels of theories predicted similar transition state geometries. The activation energy values, however, demonstrated significant dependence on the methods that were applied. All the applied "dependable" ab initio and DFT methods predicted that the breakage of the S530 Oγ—Hγ and formation of the Oγ—C(acetylsalicylic acid carbonyl) bonds occur in a single elementary step.

1. Introduction

The first commercially available synthetic antipyretic, analgesic and anti-inflammatory drug was aspirin (acetylsalicylic acid or ASA), which was commercially distributed by the end of the 19th century by Bayer. It was proposed later that aspirin suppresses prostaglandin generation in a manner similar to other non-steroidal anti-inflammatory drugs [1–3]. Because aspirin suppresses prostaglandin H2 production, which is a precursor of thromboxane A2, a potent activator of platelets, aspirin leads to the inhibition of thromboxane A2 production in platelets. ASA achieves this effect by acetylating a single serine residue (S530) of cyclooxygenase-1 (COX-1) [4–8]. This mechanism forms the basis of the protective effect of aspirin against thromboembolic vascular events [9–12]. The exact reaction mechanism of COX-1 S530 acetylation has not been revealed by experimental methods.

COXs, also known as prostaglandin H synthases (PGHSs), are bifunctional enzymes [13–16] with two spatially distinct reaction centers that are mechanistically coupled [13–15,17]. The cyclooxygenase [18,19] center catalyze the conversion of arachidonic acid to prostaglandin G2 (PGG2, a hydroperoxide endoperoxide prostaglandin), while the peroxidase [17] reaction center is responsible for the reduction of PGG2 to prostaglandin H2 (PGH2). PGH2 is then converted to a variety of prostanglandins and thromboxane A2 by specific enzymes.

Two main isoforms of COXs, COX-1 and COX-2, have been identified, although the splice variant of COX-1 is sometimes termed as COX-3 [20]. COX-1 is known to be responsible for PGH2 production [13,14,21], which is the common starting point of prostaglandin derivatives involved in basic housekeeping functions. Although COX-2 also plays a role in several "normal" physiological processes [22], its expression is predominantly induced by pathophysiological processes, including inflammation. COX-2 is also a target of non-steroidal anti-inflammatory drugs [16,23,24].

Both COX-1 and COX-2 are membrane-bound homodimers of ~70 kDa subunits [25,26] each of which consists of a short EGF domain, a membrane-binding domain and a large C-terminal catalytic domain. Although the enzymes only share ~60% amino acid identity, their structural similarity is remarkable [15,25–27]. One of the characteristic features of COX structures is the long

* Corresponding author. Tel.: +36 52 431 956; fax: +36 52 340 011.
E-mail address: komaromi@med.unideb.hu (I. Komáromi).

1093-3263/$ – see front matter © 2013 Elsevier Inc. All rights reserved.
http://dx.doi.org/10.1016/j.jmgm.2012.12.013

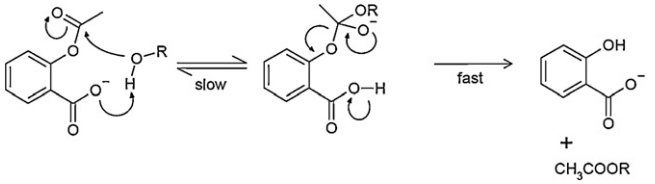

Scheme 1. General scheme for the trans-esterification reaction (R = H, alkyl, enzyme).

hydrophobic channel with an entrance at the membrane-binding domain. The active site sits at the bottom of the channel. Residues R120, Y355 and E524 separate the active site from the entrance to the channel. The structure-based residue numbering scheme generally applied to both isoforms of cyclooxygenases corresponds to sheep COX-1, from which the first COX 3D structure was resolved [25]. Despite the high structural and sequential similarity at the active site regions, the shapes of the corresponding substrate binding cavities in COX-1 and COX-2 are somewhat different [22,27–29], allowing the possibility for the development of selective COX inhibitors [23,30–35].

It was noted that the reaction of ASA with nucleophilic reagents occurs via a direct nucleophilic attack on the phenolic ester carbonyl carbon atom (Scheme 1) instead of via an anhydride intermediate [36–38]. The same mechanism appears to be straightforward for the ASA–COX reaction as well. Molecular modeling using the SCC-DFTB method in QM/MM dynamics supports this assumption [39]. From these molecular dynamics simulations and the subsequent analysis of the reaction path by B3LYP/6-31G(d) DFT calculations Tosco et al. found that first a stable hydrogen bond forms between the hydroxyl group of Y385 and the carbonyl oxygen of the acetyl group of ASA. This hydrogen bond formation orients the S530 Oγ—Hγ bond in such a way that the Hγ can migrate to the ASA carboxylate oxygen which is followed immediately by the acetyl migration from the ASA to the S530 through a tetrahedral intermediate. It was not discussed, however, whether this tetrahedral intermediate exist as a local energy minimum on the reaction path or it can be regarded rather as a point on this path which has certain geometrical parameters.

Several amino acid residues of COX-1 and COX-2 were found to be essential in the ASA–COX interactions leading to the trans-esterification reaction. Experiments using ^{14}C-acetyl-labeled aspirin with the wild-type and the point-mutated COX-2 enzyme revealed that the role of Y385 is crucial, while R120 and Y348 influence the trans-esterification reaction to a somewhat lesser extent [8]. Interestingly, Y385 also plays an essential role in the cyclooxygenase reaction, while the Y348F, Y355F and R120A mutations only partially suppress cyclooxygenase activity [40]. The X-ray structure [26] of the complex of the acetylated enzyme and the product, salicylic acid, demonstrate that salicylic acid is ~5 Å away from its "ideal" transition-state position. This finding suggests that the role of R120 is to ensure the proper orientation of ASA, rather than to directly participate in the reaction.

Despite the tremendously efficient computers and computational chemistry software available nowadays, computational studies on enzyme mechanism remains still one of the most challenging tasks. The problem resides in the fact that theoretical description of enzyme reaction mechanism would require high level computation for a large system (including the enzyme, substrate, solvent molecules, ions, etc.) for a proper description of the biochemical reaction and dynamical or Monte Carlo approach for sampling. Hybrid methods, where quantum chemistry is applied for the part of the system where the reaction takes place and low level empirical force field is used for the rest of the system in principle can give a good estimation for the characteristic features of the enzyme reaction [41–46]. However, owing to the huge number of calculations required by proper sampling, high level quantum chemistry calculation still cannot be used in these computations routinely.

To resolve this conflict a more approximate (specially parameterized) quantum chemical methods can be used for dynamical description of enzyme reaction [45,46]. Using higher level quantum mechanics calculations in non-dynamical calculations is a frequently applied complement approach to obtain information on the shape of potential energy surface of this type of reactions [41,43]. The combination of these approaches also generally accepted to gain more realistic picture and more quantitative model [39,46].

Regarding the COX enzymes besides the QM/MM dynamical studies on the aspirin trans-esterification reaction [39] only a static QM/MM study on the arachidonic acid cyclooxygenation has been found in the literature [47]. In the latter paper the initial hydrogen abstraction activation free energy was calculated in an excellent agreement with the experimental value.

Even though the ASA–COX reaction mechanism proposed by Tosco et al. [39] appears reasonable, it requires validation by sophisticated theoretical and/or experimental methods. Therefore, the goal of this study was to characterize the reaction mechanism of the irreversible inhibition of cyclooxygenase-1 by aspirin using static ONIOM type QM/MM methods. While "high level" ab initio and DFT calculations on a model system were intended to use the aim was to account for the steric and electrostatic effects of the neighboring amino acids in a relatively large surrounding region as well. The latter was achieved by using the electronic embedding method [48] in ONIOM [49,50], which allows polarizing the wave function by the surrounding partial charges. A further aim was to determine the "exact" transition state(s) and local minima on the potential energy surface and prove their existence by vibration analyses.

In addition, HF, B3LYP, B97-D and MP2 calculations using 6-31G, 6-31G(d), 6-31G(d,p) and, in a few cases, 6-31G+(d,p) basis sets were carried out to assess the dependency of the results on the level of theories applied in quantum chemical calculations. We intended to decide whether the above methods predicted a single-step elementary reaction or one of multiple steps, connecting the ASA–COX-1 complex to the salicylic acid and acetylated COX-1 product. As we plan to study the effects of point mutations in COX-1 on the ASA- human COX-1 reaction in the future, we carried out the calculations on the model of human COX-1.

2. Methods

2.1. Homology modeling and docking

As there was no experimental atomic resolution 3D structure available for the human COX-1 enzyme, it was derived using the ovine COX-1 (PDB ID 2AYL [51]) as a template by means of the YASARA software [52]. The side-chain rotamer network was optimized considering electrostatic and packing interactions. A simulated annealing type minimization with explicit solvent molecules was also carried out according to the homology modeling protocol implemented in the YASARA software. ASA was then docked to the active site of human COX-1 using the graphical interface of Autodock 4.0 software [53], Lamarckian genetic algorithm [54] was applied using a rigid receptor–flexible ligand protocol with a 0.177 Å grid spacing distance for a grid box ($98 \times 98 \times 122$ grid points) centered at S530 Oγ. The atom-specific affinity at these points were calculated by means of the autogrid 4 software. Both the autogrid 4 and autodock 4 are included in the autodock suite of docking tools. The number of hybrid GA-LS calculations, the number of individuals in the population and the maximum number of

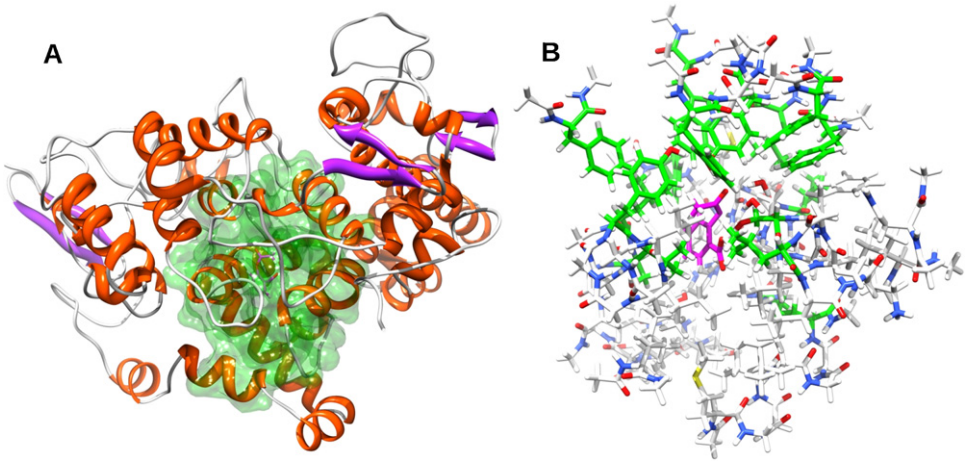

Fig. 1. (A) The whole human COX-1 enzyme derived in this work and the subsystem considered in our calculations are shown by cartoon-type and transparent surface representations, respectively. (B) The stick representation of the subsystem corresponds to the transparent surface in Fig. 1A, on which ONIOM-type QM/MM calculations were carried out. ASA is shown in violet, while the residues for which relaxation was allowed during optimization are represented by a green carbon skeleton.

energy evaluations were set to 100, 150 and 25,000,000, respectively. The other parameters were kept at their default values.

2.2. Constructing the model for QM/MM calculations

The surrounding region of the reaction center was selected as a set of residues which had at least one atom located less than 7 Å from either the S530 Oγ or the ASA carbonyl C atoms. This selection resulted in 23 residues. The actual surrounding region was much larger because additional 23 amino acids which were close to the reaction center and/or to the ASA, especially if they have polar/charged side chain, were picked out visually as well. There were no residues neglected with charged or polar side chains in the vicinity, closer than 12 Å to reaction center. When the size of the gap between the residues selected these ways were equal or less than two residues, the gap was substituted by (one or two) glycine residues. When the gaps were longer than two residues, the open N- and C-ends of the chain fragments were closed (capped) by either acetyl or N-methyl groups, respectively. The selected region featured 81 residues, including 61 "real" amino acids and 20 acetyl and N-methyl groups (Fig. 1A). The Protein Data Bank (PDB) files were converted to the Gaussian style of input files with the AMBER force field atom type and corresponding partial charges [55] by means of a small utility program that was written for this purpose.

Two main input groups were created for the 81 residues. In the first one (model A), only the S530 and Y385 side chains and the ASA molecule were allowed to relax during optimization. The inner layer, on which high-level (i.e., quantum mechanical) calculations were carried out, comprised only ASA and the side chain of S530. In the second series of calculations (models B), the side chains of R120, F198, F205, F209, Y348, V349, L352, S353, F381, L384, Y385, W387, F518, I525, L534 and the whole S530 residue as well as the ASA molecule were 'active' during geometry optimization, while all the other atoms were clamped (Fig. 1B). At this case the selection criteria for the inner (QM) layer were that the whole S530 residue, the whole ASA and side chains which form H-bond with the reaction center should be included in QM calculations. Therefore, the inner layer in this group comprised the side chain of Y385 as well. In addition, for QM calculations the S530 was completed (capped) with the acetyl and N-methyl groups replacing the preceding and following residues, respectively (Fig. 2A). The effect of other nearby residues was taken into account partially at high level in a way that their partial charges polarized the 1e Hamiltonian of the QM layer (electronic embedding).

In spite of its highly hydrophobic character, X-ray crystallography frequently reveals structural water(s) inside the substrate binding channel of COX enzymes (see structures with PDB identifiers 2AYL, 1Q4G, 1EQG). Therefore, calculations were also carried out on models that included one or two water molecules close to the S530 residue. It was presumed that water molecules contribute either to the stability of the transition state or to the proton transfer from S530 Oγ (Fig. 2A). The model B was then divided into four subgroups. In model B1, no water was included in the calculations, while models B2 and B3 contained one water molecule, and in model B4, both water positions were filled. When water molecules were included in the calculations they were always calculated at high (QM) level.

Besides, models B1′, B2′, B3′ and B4′ were created from the corresponding B1, B2, B3 and B4 models allowing all the residues listed above and additionally the H90, V345, I346, Y356, L360, I523, G526, A527, P528, F529, L531 ones to move freely during optimization. Moreover, the M113, V116, L117, I123, T206, M522, E524 and L535 residues were fixed only by their peptide bonds at B1′. . .B4′ systems.

2.3. QM/MM calculations

A series of ONIOM-type [56] QM/MM [49,50] calculations applying electronic embedding approximations were carried out at HF,

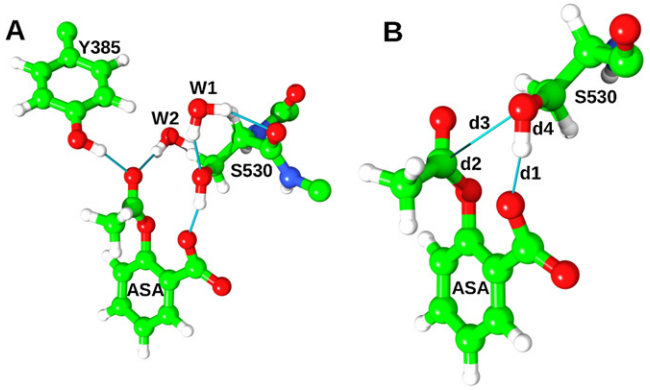

Fig. 2. (A) The subsystem on which "high level" (i.e., quantum mechanical) calculations were carried out in the ONIOM method. The two water positions we considered are marked by W1 and W2. (B) Four representative distances used in the characterization of the stationary points of the ASA–COX reaction.

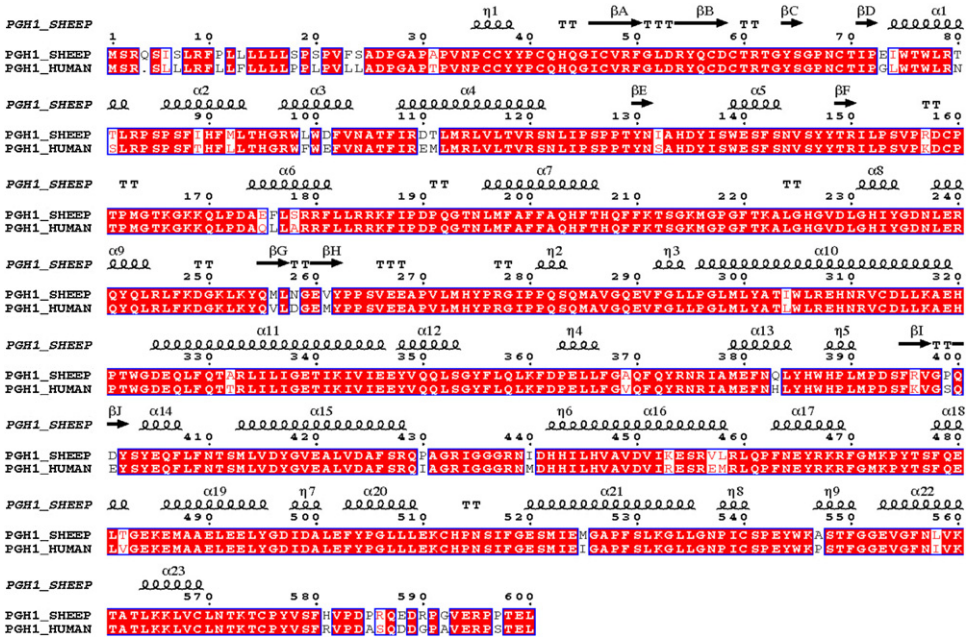

Fig. 3. Sequence alignment of sheep and human cyclooxygenase-1 (COX-1) enzymes. The secondary structure elements obtained from the sheep COX-1 X-ray structure are also shown. The β-strands are marked by bands with arrows, while helical structural elements are shown as spring-like figures.

B3LYP, MP2 and B97-D levels of theories spanning the basis sets from 6-31G to 6-31G(d,p), in a few cases to 6-31+G(d,p). Calculations on model A were carried out to map the potential energy surface as a function of the two main internal coordinates, the distance of the breaking S530 Oγ—Hγ bond and the forming Oγ—C (acetyl carbonyl of ASA) bond (*d*3 and *d*4 distances in Fig. 2B). In subsequent calculations, the selection of starting geometries for the transition state search was based on the shape of the potential energy surface.

For model B1, calculations were carried out at the HF, B3LYP and MP2 levels of theories using different kinds of standard basis sets. For the model of the ASA–COX-1 complex, the transition state and the "product" optimized geometries were determined at each level of theories that were considered. Zero point vibration energy (ZPVE) corrections to these energy values were calculated at all but the MP2, HF/6-31+G(d,p) and B3LYP/6-31+G(d,p) levels. The existence of first order saddle points and the local energy minima were proven by the analytically calculated one or zero imaginary frequencies. The first local minimum found by the optimizer after the breaking of the C (carbonyl of ASA)—O (phenolic) bond was regarded as the product. For models B2, B3 and B4 only B3LYP calculations were carried out.

B3LYP/6-31G(d) calculations for B1′...B4′ systems were compared to those obtained for B1...B4 ones in order to examine how the more extended set of variables influences the corresponding geometries and energies. Grimme's [57] B97-D functional was shown [58] to perform well even for intermolecular dispersion forces. Density functional calculations for B1′...B4′ systems using B97-D functional were also carried out from which an estimation on the dispersion energy correction was expected to obtain. These calculations, however, require considerably more optimization steps therefore require considerably longer CPU time. Moreover, the probability that the systems fall into a local energy minimum "trap" during minimizations is also increased. Therefore, only one series of these calculations, using 6-31G(d) basis, were performed.

The calculations were carried out using the Gaussian 03 [59] and Gaussian 09 [60] software suites. Visualizations were performed by the Molekel [61], Chimera 1.4 [62], VMD 1.9 [63], DPlot [64] and ESPript [65] software packages. Models B1(B1′), B2(B2′), B3(B3′) and B4(B4′) comprised 988, 991, 991 and 994 atoms, respectively, while the QM sub-system without water and with one and two water molecules comprised 56, 59 and 62 atoms, respectively. The characteristic geometry parameters of the reaction we studied are shown in Fig. 2B.

3. Results and discussion

3.1. Homology modeling and docking

The overall residue identity between ovine and human COX-1 is excellent (more than 90% with additional ∼3% residue similarities), which very likely means a correct predicted structure (Fig. 3). Especially high residue identity can be seen at and near the catalytic site of COX-1. The deletion of the Gln residue at the 4th position in sheep COX-1 is a characteristic difference between the human and the sheep enzymes, which explains why the residue numbers of human COX-1 above this position can be obtained by subtracting 1 from the sheep COX-1 residue numbers. As is typical in the structural studies of COX enzymes, the sheep COX-1 numbering convention will be used throughout this work. The homology modeling protocol of YASARA includes both simulated annealing type minimization using explicit solvent molecules and side chain optimization procedure. Owing to these optimizations the homology modeling finally resulted in a ∼0.53 Å rms deviation between the template (X-ray) and the target (theoretical) structure. The proposed protein structure obtained this way was validated using both the PROCHECK [66] and the verify3D [67,68] software tools. Validations showed that the formal quality of proposed human COX-1 structure is at least as good as the original template 2YAL PDB structure. Because of the facts mentioned above and because of the existing functional identity between the target and the template COX-1 enzymes, no additional molecular dynamics simulations was carried out to check the stability of the target structure.

The docking protocol resulted in practically two orientations for the ASA in complex with COX-1. The most stable and most populated pose one (∼70%) obtained by docking the aspirin to the active site resulted in a complex suitable for the next step of the reaction. In this orientation, the S530 Oγ atom is sufficiently close to the

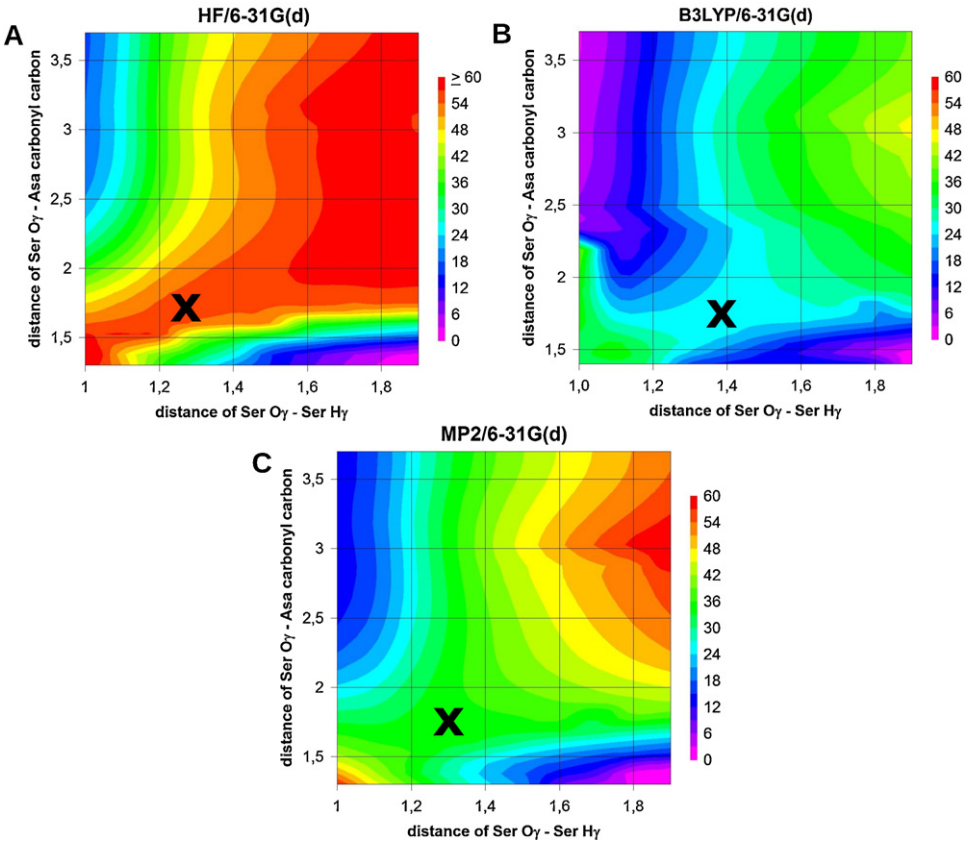

Fig. 4. The ONIOM(HF/6-31G(d):AMBER) (A), ONIOM(B3LYP/6-31G(d):AMBER) (B) and the ONIOM(MP2/6-31G(d):AMBER) (C) potential energy surfaces as the function of S530 Oγ–S530 Hγ and the S530 Oγ–C (ASA acetyl carbonyl) distances. The approximate positions of saddle points on the surfaces are marked by "x".

carbonyl carbon of the ASA acetyl group for a nucleophilic attack, while the S530 Hγ is close to the carboxylate oxygen, which may help the Hγ atom to leave the S530 Oγ atom. The other, less stable orientation was populated in a less degree (∼30%). It did not correspond to a position which was required for the trans-esterification reaction. It should be mentioned that upon carrying out the same docking with different docking parameters, the most stable pose obtained by Tosco et al. [39] corresponded to an ion-pair between the ASA and the R120 residue. They found the orientation derived in this work only the 2nd most stable one. The reason for this disagreement can be that the docking box applied in this study was very likely smaller than those one applied by Tosco et al. Nevertheless, both poses should have considerable statistical probabilities. The ion-pair formation may play a role in the pre-orientation of ASA in the substrate-binding channel, while the other orientation is required for the trans-esterification reaction. This latter one was accepted as a starting geometry for the ASA–COX-1 reaction. The geometry of this complex was optimized but no additional molecular dynamics simulations were carried out.

3.2. Potential energy surfaces

In the case of the simpler model (model A), the potential energy surfaces as a function of the S530 Oγ–C (ASA acetyl carbonyl) and the S530 Hγ–S530 Oγ distances suggested only a single saddle point for all the ONIOM QM/MM calculations (Fig. 4A–C). The approximate positions of these points are marked by "x" on the maps. Nevertheless, the shapes of the potential energy surfaces differ slightly from each other. On the surface calculated by the B3LYP/6-31G(d):AMBER method, a relatively narrow valley leads to the saddle point. Neither the HF/6-31G(d):AMBER nor the MP2/6-31G(d):AMBER surface shows a similar property. There is no sign of a distinct reaction step for the Hγ proton transfer from the Oγ atom to the ASA carboxylate and the nucleophilic attack of Oγ on the ASA carbonyl carbon atom. Based on these maps, it seems that the transition state (TS) features a relatively short Oγ–Hγ distance. The potential energy surfaces at or near the saddle point appear to be remarkably flat. This indicates that even small perturbations can cause relatively large shifts in the position of the TS. Based on these maps, it can also be summarized that when the ASA is non-covalently bonded to the COX-1 enzyme, it has reasonably large freedom to move without any considerable energy barriers. Therefore, its carbonyl carbon atom can easily approach the S530 Oγ atom, allowing the nucleophilic attack to take place.

3.3. Geometry of the stationary points

The reaction centers of the ASA–COX-1 complex, the transition state, and the acetylated COX-1–salicylic acid complex are shown in our model B1 (Fig. 5A–C). In the ASA–COX-1 complex model (obtained from the docked pose by geometry optimization), a characteristic hydrogen bond (*d*1, see in Fig. 2B) exists between S530 Hγ and one of the O atoms of the ASA carboxyl group (Table 1). The Hγ proton is bonded at each level of theory that was applied to the Oγ atom (*d*4 in Fig. 2B). The bond between the phenolic O and the carbonyl C has the usual, ∼1.35 Å bond length. The separation between the bridge atoms of the newly formed bond (i.e., between S530 Oγ and carbonyl C of the acetyl group in ASA, see *d*3 in Fig. 2B) is approximately 3.5 Å; this value only slightly depends on the applied QM/MM method. This value appears to be slightly too long for a subsequent reaction. It was shown, however, that these bridge atoms can approach each other without experiencing any significant energy barriers.

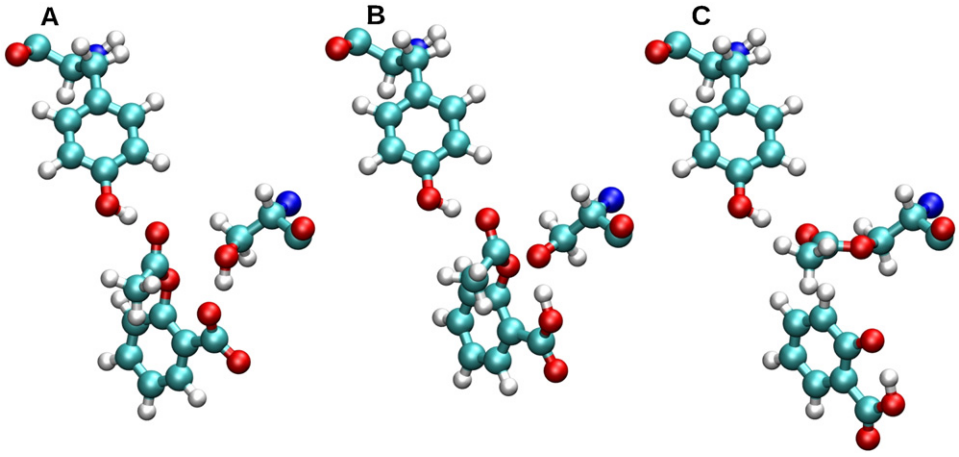

Fig. 5. Representative examples for the position of ASA and the Y385 and S530 residues in the ASA–COX-1 complex (A), transition state (B), and acetylated COX-1, salicylic acid product (C) geometries.

Regarding the transition state geometry parameters we obtained (Figs. 2B and 5B), it is interesting to observe that the S530 Hγ proton–ASA carboxylic O distances are close to a normal O—H bond length, while the S530 Hγ–Oγ distances are much longer. It seems as if the proton transfer would precede the O—C bond formation. The distances for the newly formed O—C bond are in the range of 1.7–1.9 Å. Investigating the effects of the basis set alone, substantially fewer variations were observed in the geometry parameters. It is also worth mentioning that the (phenolic) O—C (acetyl carbonyl) bond was elongated remarkably in the transition state. This is not surprising, as the breaking of this bond yields the final product.

Concerning the product geometries (Figs. 2B and 5B), noteworthy variations can be observed in the geometry parameters (S530 Hγ–S530 Oγ and phenolic O–acetyl carbonyl C distances) associated with the movement of salicylic acid from the transition state. While at the MP2 level, the salicylic acid moves away a little from the reaction center, its dislocation is remarkable at the HF levels using all but the 6-31G basis. Using the 6-31G(d) and 6-31G(d,p) basis sets, salicylic acid is closer to the position observed by previous X-ray experiments for the product geometry [26]. B3LYP methods resulted in distances that are between those obtained by the other two applied methods. It is important to note that the proton position situated on one of the carboxylic oxygens of salicylic acid is in agreement with the position demonstrated in an earlier modeling study [39]. Theoretical considerations and experimental findings [26] suggest that the proton needs to migrate to the phenolic oxygen. The migration can be prevented by either an energy barrier or by a higher energy for the carboxylate tautomer. Even the latter case cannot be excluded in the protein environment, as was observed during the QM/MM dynamics simulation using the SCC-DFTB method at the QM level [39]. The possibility that the result might be an artifact of the SCC-DFTB method was excluded; after re-optimization of the two isolated tautomers by the B3LYP/6-31G(d) method, the phenoxy form was found to be a more stable conformation.

3.4. Activation energies

The results obtained for transition states in the model B1 system by ONIOM-type QM/MM calculations are summarized in Table 1. Applying HF "high level" calculations, the activation energies (i.e., the energy differences between the ASA–COX-1 complex and the transition state models) are systematically higher than those obtained by either B3LYP density functional or by MP2 calculations. This is not surprising, as HF methods neglect the correlation energy that is considerably higher at the transition states than at "normal" bonding conditions [69–71]. The effect of the basis sets we applied has less importance, except when the first set of polarization functions to the non-hydrogen atoms are added. Including the ZPVE correction in the calculation of activation energies resulted in lower values (up to 2 kcal/mol), depending on the level of theory we applied.

The energy differences between the ASA–COX-1 complex and the complex between salicylic acid and acetylated COX-1 were also calculated. As shown in Table 1, independent of the method we used, the product always had substantially lower energy (i.e., it was more stable) than the ASA–COX-1 complex. Therefore, the inverse reaction pathway has negligible probability. This finding is in agreement with the irreversible nature of inhibition [16,72] and the earlier modeling results [39].

We were not able to find any experimental value for the activation energy in the existing literature. Tosco et al. demonstrated that the QM/MM calculation applying the SCC-DFTB QM method most likely underestimates the activation energy [39]. Using B3LYP/6-31G(d) to correct the SCC-DFTB potential energy surface, they found the activation free energy to be ∼10 kcal/mol. Our calculations resulted in comparably higher ZPVE corrected activation energy values (∼20–22 kcal/mol at density functional- and MP2 levels of theories). The reason for this discrepancy may be caused by the difference in the computational models used. In this work the exact transition state geometry were aimed to determine at different levels of theories when only a subsystem of COX-1 was allowed to relax during geometry optimization. The model used in this study is very likely more suitable for the initial complex than the transition state. The simple optimization (transition state search) method finds the optimal geometry of the latter one using the constraints applied in the initial complex. Tosco et al. modeled the dynamical reaction path of the trans-esterification reaction, applying a more approximate QM method in QM/MM calculations, which allowed the entire COX-1–ASA system to be included in the dynamical simulation.

3.5. Imaginary vibrations

In every case, only a single imaginary frequency was obtained for the transition state, and all frequencies for the geometry of ASA–COX-1 and salicylic acid – acetylated COX-1 complexes were positive. The normal mode corresponding to the imaginary frequency (Fig. 6) shows that the proton migration between S530 Oγ and ASA carboxylate O atoms and the bond breakage/formation

Table 1
Representative distances *d1*, *d2*, *d3* and *d4* distances (see Fig.2) [Å] and relative energy values [kcal/mol] of the stationary points found at the B1 model of ASA–COX-1 reaction calculated at different levels of theories. The TS-Complex (i.e. ASA–COX-1 complex) and TS-Product (i.e. complex of salicylic acid and acetylated-COX-1) activation energies correspond to the forward and backward reactions. The ZPVE corrected values are also given.

Methods	Basis	ASA–COX-1 complex				ASA–COX-1 TS				ASA-acetyl-COX-1				TS-Complex		TS-Product	
		d1	*d2*	*d3*	*d4*	*d1*	*d2*	*d3*	*d4*	*d1*	*d2*	*d3*	*d4*	TS-C	TS-C ZPVE	TS-P	TS-P ZPVE
HF	6-31G	1.735	1.349	3.522	0.968	1.091	1.444	1.775	1.309	0.993	4.333	1.335	3.284	32.92	30.32	44.34	43.27
	6-31G(d)	1.806	1.328	3.526	0.960	0.995	1.417	1.872	1.603	0.986	7.212	1.323	6.202	40.16	39.48	59.89	60.48
	6-31G(d,p)	1.809	1.328	3.521	0.956	1.002	1.415	1.814	1.529	0.987	7.206	1.323	6.216	40.01	39.12	60.11	60.50
	6-31+G(d,p)	1.847	1.329	3.526	0.955	1.006	1.417	1.821	1.513	0.985	7.168	1.322	6.171	42.59	41.70[a]	64.18	64.57[a]
B3LYP	6-31G	1.638	1.376	3.446	1.044	1.086	1.536	1.740	1.372	1.071	4.536	1.357	3.654	18.59	17.13	34.78	35.16
	6-31G(d)	1.699	1.352	3.476	0.991	1.055	1.479	1.790	1.448	1.040	5.333	1.341	4.372	24.35	22.21	40.01	39.77
	6-31G(d,p)	1.682	1.352	3.467	0.990	1.052	1.495	1.736	1.433	1.052	5.083	1.340	4.180	23.77	21.28	39.80	39.24
	6-31+G(d,p)	1.725	1.354	3.456	0.986	1.054	1.513	1.704	1.434	1.090	6.965	1.347	6.236	27.05	24.56[b]	50.94	50.38[b]
MP2	6-31G	1.713	1.399	3.395	1.001	1.089	1.552	1.807	1.407	1.057	4.699	1.378	3.728	22.74	20.25[b]	32.30	31.74[b]
	6-31G(d)	1.708	1.358	3.368	0.992	1.095	1.470	1.801	1.370	1.050	3.989	1.345	2.978	24.31	21.82[b]	34.47	33.91[b]
	6-31G(d,p)	1.664	1.359	3.313	0.987	1.076	1.481	1.752	1.372	1.062	3.888	1.346	2.927	23.42	20.93[b]	33.63	33.07[b]

[a] Corrected by the ZPVE difference calculated at HF/6-31G(d,p) level of theory.
[b] Corrected by the ZPVE difference calculated at B3LYP/6-31G(d,p) level of theory.

between S530 Oγ and carbonyl carbon of the ASA acetyl group occur in the same elementary step even if they are not fully synchronous events. Considering that in the transition state, the Hγ proton migration to the ASA carboxyl group is almost completed, this is an interesting result.

3.6. Existence of the tetrahedral intermediate

The first step of the reaction resembles the nucleophilic attack on peptide carbonyl by the serine Oγ atom in serine proteases. By analogy a question arose which concerns the existence of the so-called tetrahedral intermediate. In this case, a local minimum on the potential energy surface should exist, corresponding to an already-formed Oγ—C(ASA—carbonyl) bond with a simultaneously existing phenolic O—C(ASA—carbonyl) bond (Scheme 1). Interestingly, our efforts to find this intermediate failed. Optimizations started from geometries, which were taken from the product side but not too far from the saddle point, resulted in the final product geometry. Although these type of calculations cannot be regarded as an exact proof of the non-existence of the tetrahedral intermediate, they are a good estimation that the intermediate, should it exist, would have a small energy barrier to prevent bond splitting.

3.7. Position of the negative charge on the salicylic acid

We found that even after the trans-esterification reaction had been completed, the S530 Hγ proton was bonded to the carboxylic oxygen of the newly formed salicylic acid. Because in water at near-neutral pH values, the proton should be on the phenolic O instead of the carboxylic O [73], the same was expected for the system we studied. Nevertheless, one must consider that the electrostatic field of proteins can considerably influence the environment. Therefore, a relaxed potential energy scan moving the proton from the carboxylic oxygen to the phenolic oxygen was carried out, and the potential energy curve was calculated at the B3LYP/6-31G(d):AMBER level (Fig. 7). The protein electrostatic field was taken into consideration using the electronic embedding method and was applied throughout the study. Fig. 7 shows that the proton prefers to stay near the phenolic oxygen even if the energy gain is not especially large. The energy barrier purported to prevent the movement of the proton from the carboxylic oxygen is very low, less than 0.5 kcal/mol. This barrier can easily be overcome by thermal motion.

3.8. A possible effect of water molecules on the reaction

As mentioned above, structural (i.e., with resolved oxygen position) waters are frequently found in the COX-1 substrate-binding cavity via X-ray analysis. This discovery raised the question of whether ASA leaves room for water molecule(s) in the channel and, if this is the case, whether this/these molecule(s) can influence the reaction mechanism and/or the activation energies. To answer these questions, we carried out calculations for models B2, B3 and B4. In this case, only the B3LYP method with different basis sets was used as a high level theory in the ONIOM computations. The results are summarized in Table 2.

In model B2, the water molecule is in a position that can form an H-bond with the Oγ atom; therefore, we expect that it can facilitate the proton transfer from Oγ (W1 in Fig. 2A) to the ASA carboxylate. Despite the easier proton transfer from the Oγ atom, the activation energy remains approximately the same (or a little higher if using the 6-31G basis) as it was in the case when water was omitted from the calculation (model B1). One possible interpretation of this result is that in the transition state, the proton is almost completely transferred to the ASA carboxylate, even in model B1. The new H-bond between the water and the S530 Oγ contributes only marginally to

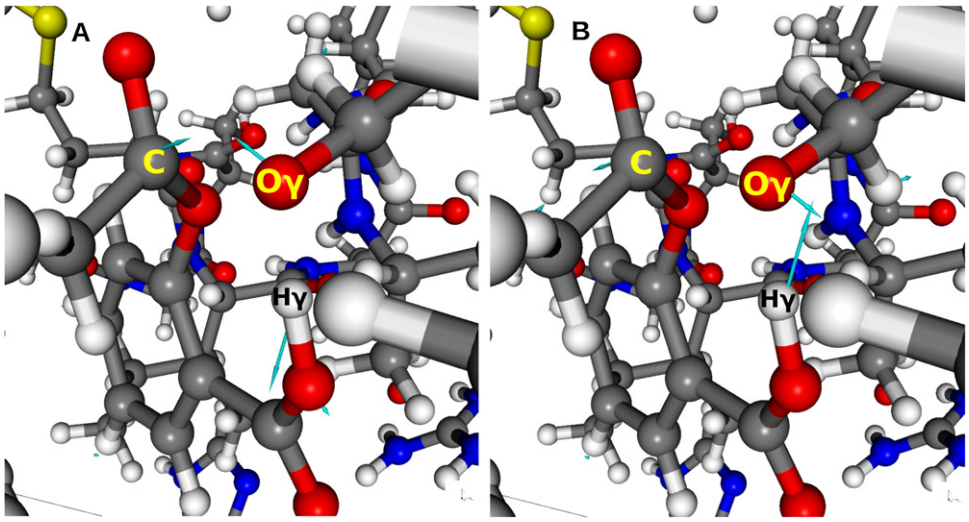

Fig. 6. The vibration mode corresponding to the imaginary frequency at the transition state calculated by the ONIOM(B3LYP/6-31G(d):AMBER) level of theory. The ASA acetyl carbonyl carbon, the S530 Oγ and S530 Hγ atoms are marked by C, Oγ and Hγ, respectively. The vibration mode is shown in light-blue arrows. Parts A and B of figure represent the forward and backward directions on the reaction path.

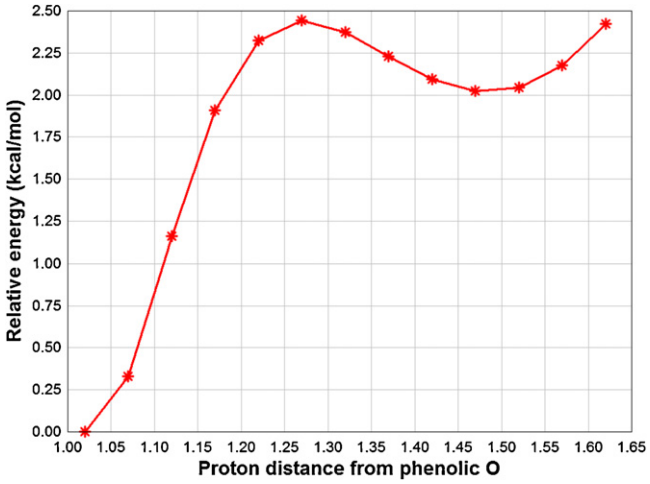

Fig. 7. Potential energy graph as a function of proton distance from the phenolic O of salicylic acid in the "product" geometry, calculated by the ONIOM(B3LYP/6-31G(d):AMBER) level of theory.

that process. Even this contribution can be compensated because the H-bonded water decreases the nucleophilicity of the S530 Oγ, which can cause slightly increased activation energy. In the transition state, the Ser Oγ—Hγ bond length is more elongated than in model B1. The calculations show that this water molecule does not considerably influence the geometric parameters of the ASA–COX-1 non-bonding complex state (Table 2).

In model B3, the water molecule occupies a position where it can form a H-bond with the carbonyl oxygen of the ASA acetyl group (W2 in Fig. 2A). Because it is presumed that the transition state resembles a tetrahedral intermediate, the additional H-bond may stabilize the transition state. In fact, the Tyr385 residue is found to be essential in the ASA–COX trans-esterification reaction [8]. We examined this hypothesis by a series of calculations, using the B3LYP method in ONIOM as a high-level calculation. Our results do not support this presumption (Table 2) because in this case, the effect of H-bond stabilization on the transition state energies and geometries was only marginal. Similar to the previous results, when two water molecules (in both of the positions mentioned previously) were included in the calculations (model B4), neither the transition state geometry nor the activation energy was substantially influenced.

Table 2
Representative *d*1, *d*2, *d*3 and *d*4 distances (see Fig. 2) [Å] and relative energy values [kcal/mol] for the B2, B3 and B4 model of ASA–COX-1 complex and the transition state calculated by B3LYP DFT method using different basis sets. The activation energies as the difference of transition state (TS) energy and the energy of ASA–COX-1 complex (C) are given along with their ZPVE corrected values.

System	Basis	ASA–COX-1 complex				ASA–COX-1 TS				TS-C	TS-C ZPVE
		*d*1	*d*2	*d*3	*d*4	*d*1	*d*2	*d*3	*d*4		
B2	6-31G	1.560	1.379	3.433	1.016	1.200	1.531	1.730	1.400	25.02	22.01
	6-31G(d)	1.622	1.354	3.462	1.001	1.006	1.513	1.756	1.677	24.18	23.44
	6-31G(d,p)	1.591	1.354	3.449	1.001	1.003	1.531	1.708	1.656	24.41	23.61
B3	6-31G	1.664	1.367	3.546	1.003	1.111	1.495	1.777	1.327	18.42	16.80
	6-31G(d)	1.723	1.344	3.546	0.990	1.072	1.449	1.831	1.409	24.63	22.80
	6-31G(d,p)	1.712	1.344	3.542	0.988	1.069	1.460	1.780	1.398	24.02	22.36
B4	6-31G	1.590	1.370	3.565	1.013	1.029	1.533	1.720	1.550	20.48	19.44
	6-31G(d)	1.655	1.346	3.555	1.013	1.015	1.471	1.801	1.613	24.16	23.19
	6-31G(d,p)	1.632	1.346	3.550	0.997	1.013	1.484	1.746	1.591	24.28	23.27

Table 3
Representative distances *d*1, *d*2, *d*3 and *d*4 distances (see Fig. 2) [Å] and relative energy values [kcal/mol] for the B1′, B2′, B3′ and B4′ model of ASA–COX-1 complex and the transition state calculated by B3LYP and B97-D DFT methods using 6-31G(d) basis set. The activation energies as the difference of transition state (TS) energy and the energy of ASA–COX-1 complex (C) are given along with their ZPVE corrected values.

System	Basis	ASA–COX-1 complex				ASA–COX-1 TS				TS-C	TS-C ZPVE
		*d*1	*d*2	*d*3	*d*4	*d*1	*d*2	*d*3	*d*4		
B1′	B3LYP/6-31G(d)	1.694	1.352	3.514	0.992	1.058	1.466	1.823	1.448	23.89	22.05
B1′	B97-D/6-31G(d)	1.669	1.362	3.312	0.999	1.042	1.515	1.787	1.526	20.17	19.00
B2′	B3LYP/6-31G(d)	1.616	1.354	3.507	1.002	1.007	1.492	1.800	1.683	23.31	22.41
B2′	B97-D/6-31G(d)	1.578	1.365	3.303	1.013	1.003	1.547	1.778	1.769	19.06	18.55
B3′	B3LYP/6-31G(d)	1.715	1.345	3.629	0.991	1.068	1.442	1.849	1.422	25.2	23.30
B3′	B97-D/6-31G(d)	1.708	1.353	3.451	0.997	1.046	1.481	1.808	1.515	21.16	20.21
B4′	B3LYP/6-31G(d)	1.650	1.357	4.011	1.004	1.012	1.463	1.821	1.640	24.78	23.78
B4′	B97-D/6-31G(d)	1.621	1.355	3.464	1.008	1.004	1.513	1.766	1.743	20.02	19.59

3.9. The effect of extended geometry optimization and the dispersion corrected density functional

B3LYP/6-31G(d) optimization for the B1′, B2′, B3′ and B4′ systems were carried out in order to examine how the relaxation of the extended set of amino acids influences the results detailed above. In this optimization practically all but the borderline region amino acids of the B1′. . .B4′ systems and the whole COX-1 enzyme were allowed to move during optimization.

From Table 3, comparing the B3LYP/6-31G(d) results to the corresponding ones in Tables 1 and 2 it is clearly demonstrated, that the extended set of geometry variables to optimize did not change significantly either the values of the representative variables around the reaction center or the activation energy barrier of the reaction. A somewhat different situation can be observed when the results obtained using B97-D functional are compared to those that were obtained at B3LYP level of theory. The B97-D method predicts significantly lower (by ∼3–4 kcal/mol) activation energy than the B3LYP one. The corresponding geometry parameters are quite similar except the d4 values for which the B97-D sometime predicts substantially higher value. It underlines the non-negligible nature of the dispersion interaction energy terms in DFT calculations.

It should be also mentioned that an attempt to find local energy minima on the potential energy surfaces corresponding to the "tetrahedral intermediate" was also carried out for these B1′. . .B4′ systems at both the B3LYP/6-31G(d) and B97D/6-31G(d) levels of theory. Starting from the transition state geometry only the S530 Hγ atom was shifted along the S530 Oγ–Hγ or Hγ–O(ASA–acidic) interval by one tenth of the actual distance to the direction of Oγ or O(ASA–acidic), respectively. Geometry optimization started from these points resulted in, with no exception, either the initial complex or the product, respectively. This observation confirmed also that a single first order transition state connects the initial complex to the products and gave additional confirmation for the non existence of the tetrahedral intermediate-like product as we proposed above.

The result can be summarized schematically as it is shown in Fig. 8. When the ASA approaches the substrate binding cavity of the COX-1 in a proper orientation it forms an initial complex with the COX-1 enzyme. In the orientation very likely the R120 while in the proper binding the Y385 play essential role. This initial complex can be regarded as the reactants (Fig. 8). In this complex the acetyl carbonyl carbon of ASA is in a position where it can be attacked by the Oγ atom of S530 which results in a transition state shown in figure. In this TS the C(acetyl carbonyl carbon)—Oγ and O(ASA-carboxylate)—Hγ bond formation as well as the breakage of S530 Oγ–Hγ and the C(acetyl carbonyl carbon)—O(ASA-phenolic) occur in one elementary step. It should be noted that it does not mean that the bond breakages and formations are fully synchronous processes. It was demonstrated e.g. that the Hγ migration preceded the C(acetyl carbonyl carbon)—Oγ bond formation. Without any further transition state the products form in which the Oγ proton is still on the carboxylate oxygen of the salycilic acid. The Oγ proton can, however, easily migrates from the carboxylate to the phenolate oxygen. The latter process is not shown in Fig. 8.

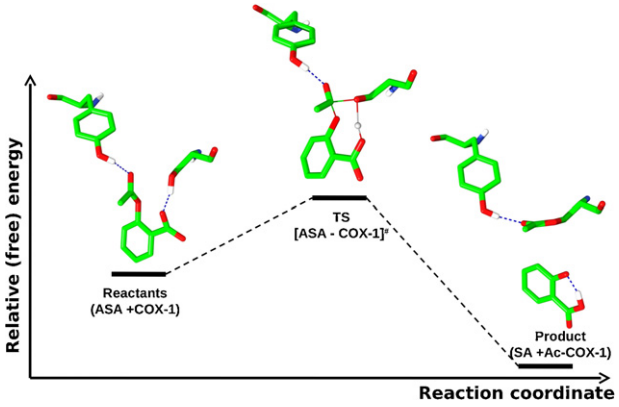

Fig. 8. Schematic representation of the ASA–COX-1 trans-esterification reaction as can be proposed based on this study. The trans-esterification reaction occurs in one elementary step where a single TS connects the reactants to the products.

4. Conclusions

The structure of human COX-1 was constructed from ovine COX-1 by homology modeling, and ASA was docked into the substrate-binding cavity of the enzyme. A series of ONIOM-type QM/MM calculations applying electronic embedding approximations were carried out at different QM levels of theories on ASA and on the surrounding amino acids to propose a plausible reaction mechanism for the ASA–COX-1 trans-esterification reaction. Within the framework of the models that were constructed for the study, the exact transition state, the local minimum geometries and the corresponding ZPVE-corrected energy values were determined. The existence of the transition state was proven by frequency analysis. By disregarding the ASA–COX-1 complex formation, we found that this reaction is essentially a single-step elementary reaction. The imaginary frequency is dominated by the S530 Hγ proton transfer and S530 Oγ—C (ASA acetyl carbon) "bond stretching" modes, which also proves the one-step elementary reaction model for proton transfer and Oγ—C bond formation.

Acknowledgments

Support was provided by the National Office of Research and Technology (Jedlik Ányos grant, NKFP-07-A1-2008-0127), the Hungarian National Infrastructure Development Program (grant: NIIF

1057), by the TÁMOP-4.2.2/B-10/1-2010-0024 project and the Hungarian Academy of Sciences (MTA 11003).

References

[1] J.B. Smith, A.L. Willis, Aspirin selectively inhibits prostaglandin production in human platelets, Nature – New Biology 231 (25) (1971) 235–237.
[2] S.H. Ferreira, S. Moncada, J.R. Vane, Indomethacin and aspirin abolish prostaglandin release from the spleen, Nature – New Biology 231 (25) (1971) 237–239.
[3] J.R. Vane, Inhibition of prostaglandin synthesis as a mechanism of action for aspirin-like drugs, Nature – New Biology 231 (25) (1971) 232–235.
[4] G.J. Roth, C.J. Siok, J. Ozols, Structural characteristics of prostaglandin synthetase from sheep vesicular gland, Journal of Biological Chemistry 255 (4) (1980) 1301–1304.
[5] G.J. Roth, N. Stanford, P.W. Majerus, Acetylation of prostaglandin synthase by aspirin, Proceedings of the National Academy of Sciences of the United States of America 72 (8) (1975) 3073–3076.
[6] G.J. Roth, C.J. Siok, Acetylation of the NH2-terminal serine of prostaglandin synthetase by aspirin, Journal of Biological Chemistry 253 (11) (1978) 3782–3784.
[7] G.J. Roth, E.T. Machuga, J. Ozols, Isolation and covalent structure of the aspirin-modified, active-site region of prostaglandin synthetase, Biochemistry 22 (20) (1983) 4672–4675.
[8] G.P. Hochgesang, S.W. Rowlinson, L.J. Marnett, Tyrosine-385 is critical for acetylation of cyclooxygenase-2 by aspirin, Journal of the American Chemical Society 122 (27) (2000) 6514–6515.
[9] J.L. Mehta, B. Mohandas, Aspirin resistance: fact or fiction? A point of view, World Journal of Cardiology 2 (9) (2010) 280–288.
[10] A. Szczeklik, J. Musial, A. Undas, M. Sanak, Aspirin resistance, The Journal of Thrombosis and Haemostasis 3 (8) (2005) 1655–1662.
[11] B. Pamukcu, A review of aspirin resistance; definition, possible mechanisms, detection with platelet function tests, and its clinical outcomes, Journal of Thrombosis and Thrombolysis 23 (3) (2007) 213–222.
[12] E.D. Michos, R. Ardehali, R.S. Blumenthal, R.A. Lange, H. Ardehali, Aspirin and clopidogrel resistance, Mayo Clinic Proceedings 81 (4) (2006) 518–526.
[13] R.J. Kulmacz, W.A. van der Donk, A.L. Tsai, Comparison of the properties of prostaglandin H synthase-1 and -2, Progress in Lipid Research 42 (5) (2003) 377–404.
[14] W.L. Smith, I. Song, The enzymology of prostaglandin endoperoxide H synthases-1 and -2, Prostaglandins and Other Lipid Mediators 68/69 (2002) 115–128.
[15] R.G. Kurumbail, J.R. Kiefer, L.J. Marnett, Cyclooxygenase enzymes: catalysis and inhibition, Current Opinion in Structural Biology 11 (6) (2001) 752–760.
[16] A.L. Blobaum, L.J. Marnett, Structural and functional basis of cyclooxygenase inhibition, Journal of Medicinal Chemistry 50 (7) (2007) 1425–1441.
[17] A.L. Tsai, R.J. Kulmacz, Prostaglandin H synthase: resolved and unresolved mechanistic issues, Archives of Biochemistry and Biophysics 493 (1) (2010) 103–124.
[18] G. Wu, J.M. Lu, W.A. van der Donk, R.J. Kulmacz, A.L. Tsai, Cyclooxygenase reaction mechanism of prostaglandin H synthase from deuterium kinetic isotope effects, Journal of Inorganic Biochemistry 105 (3) (2011) 382–390.
[19] L.J. Marnett, Cyclooxygenase mechanisms, Current Opinion in Chemical Biology 4 (5) (2000) 545–552.
[20] K.L. Roos, D.L. Simmons, Cyclooxygenase variants: the role of alternative splicing, Biochemical and Biophysical Research Communications 338 (1) (2005) 62–69.
[21] C.A. Rouzer, L.J. Marnett, Structural and functional differences between cyclooxygenases: fatty acid oxygenases with a critical role in cell signaling, Biochemical and Biophysical Research Communications 338 (1) (2005) 34–44.
[22] T. Grosser, S. Fries, G.A. FitzGerald, Biological basis for the cardiovascular consequences of COX-2 inhibition: therapeutic challenges and opportunities, Journal of Clinical Investigation 116 (1) (2006) 4–15.
[23] L. Navidpour, M. Amini, H. Shafaroodi, K. Abdi, M.H. Ghahremani, A.R. Dehpour, A. Shafiee, Design and synthesis of new water-soluble tetrazolide derivatives of celecoxib and rofecoxib as selective cyclooxygenase-2 (COX-2) inhibitors, Bioorganic and Medicinal Chemistry Letters 16 (17) (2006) 4483–4487.
[24] J.L. Masferrer, B.S. Zweifel, P.T. Manning, S.D. Hauser, K.M. Leahy, W.G. Smith, P.C. Isakson, K. Seibert, Selective inhibition of inducible cyclooxygenase 2 in vivo is antiinflammatory and nonulcerogenic, Proceedings of the National Academy of Sciences of the United States of America 91 (8) (1994) 3228–3232.
[25] D. Picot, P.J. Loll, R.M. Garavito, The X-ray crystal structure of the membrane protein prostaglandin H2 synthase-1, Nature 367 (6460) (1994) 243–249.
[26] P.J. Loll, D. Picot, R.M. Garavito, The structural basis of aspirin activity inferred from the crystal structure of inactivated prostaglandin H2 synthase, Nature Structural & Molecular Biology 2 (8) (1995) 637–643.
[27] R.M. Garavito, D.L. DeWitt, The cyclooxygenase isoforms: structural insights into the conversion of arachidonic acid to prostaglandins, Biochimica et Biophysica Acta 1441 (2/3) (1999) 278–287.
[28] M.P. Gauthier, C. Michaux, S. Rolin, C. Vastersaegher, X. de Leval, F. Julemont, L. Pochet, B. Masereel, Synthesis, molecular modelling and enzymatic evaluation of (+/−)3,5-diphenyl-2-thioxoimidazolidin-4-ones as new potential cyclooxygenase inhibitors, Bioorganic and Medicinal Chemistry 14 (4) (2006) 918–927.
[29] K.E. Furse, D.A. Pratt, N.A. Porter, T.P. Lybrand, Molecular dynamics simulations of arachidonic acid complexes with COX-1 and COX-2: insights into equilibrium behavior, Biochemistry 45 (10) (2006) 3189–3205.
[30] L. Shi, Z.L. Li, Y. Yang, Z.W. Zhu, H.L. Zhu, Design of novel N-phenylnicotinamides as selective cyclooxygenase-1 inhibitors, Bioorganic and Medicinal Chemistry Letters 21 (1) (2011) 121–124.
[31] G. Dannhardt, W. Kiefer, Cyclooxygenase inhibitors – current status and future prospects, European Journal of Medical Chemistry 36 (2) (2001) 109–126.
[32] V. Limongelli, M. Bonomi, L. Marinelli, F.L. Gervasio, A. Cavalli, E. Novellino, M. Parrinello, Molecular basis of cyclooxygenase enzymes (COXs) selective inhibition, Proceedings of the National Academy of Sciences of the United States of America 107 (12) (2010) 5411–5416.
[33] A.S. Nies, M.J. Gresser, Cyclooxygenase-2 inhibitors, Advances in Protein Chemistry 56 (2001) 115–141.
[34] R.J. Flower, The development of COX2 inhibitors, Nature Reviews Drug Discovery 2 (3) (2003) 179–191.
[35] P.A. Datar, E.C. Coutinho, A CoMFA study of COX-2 inhibitors with receptor based alignment, Journal of Molecular Graphics and Modelling 23 (3) (2004) 239–251.
[36] A.R. Fersht, A.J. Kirby, The hydrolysis of aspirin. Intramolecular general base catalysis of ester hydrolysis, Journal of the American Chemical Society 89 (19) (1967) 4857–4863.
[37] T. St Pierre, W.P. Jencks, Intramolecular catalysis in the reactions of nucleophilic reagents with aspirin, Journal of the American Chemical Society 90 (14) (1968) 3817–3827.
[38] D.S. Kemp, T.D. Thibault, The hydrazinolysis of salicyloylsalicylic acid. The irrelevance of an anhydride intermediate, Journal of the American Chemical Society 90 (25) (1968) 7154–7155.
[39] P. Tosco, L. Lazzarato, Mechanistic insights into cyclooxygenase irreversible inactivation by aspirin, ChemMedChem 4 (6) (2009) 939–945.
[40] S.W. Rowlinson, J.R. Kiefer, J.J. Prusakiewicz, J.L. Pawlitz, K.R. Kozak, A.S. Kalgutkar, W.C. Stallings, R.G. Kurumbail, L.J. Marnett, A novel mechanism of cyclooxygenase-2 inhibition involving interactions with Ser-530 and Tyr-385, Journal of Biological Chemistry 278 (46) (2003) 45763–45769.
[41] R.A. Friesner, V. Guallar, Ab initio quantum chemical and mixed quantum mechanics/molecular mechanics (QM/MM) methods for studying enzymatic catalysis, Annual Review of Physical Chemistry 56 (2005) 389–427.
[42] H.M. Senn, W. Thiel, QM/MM methods for biological systems, Atomistic Approaches in Modern Biology: From Quantum Chemistry to Molecular Simulations 268 (2007) 173–290.
[43] H.M. Senn, W. Thiel, QM/MM methods for biomolecular systems, Angewandte Chemie-International Edition 48 (7) (2009) 1198–1229.
[44] M. Mladenovic, R.F. Fink, W. Thiel, T. Schirmeister, B. Engels, On the origin of the stabilization of the zwitterionic resting state of cysteine proteases: a theoretical study, Journal of the American Chemical Society 130 (27) (2008) 8696–8705.
[45] O. Acevedo, W.L. Jorgensen, Advances in quantum and molecular mechanical (QM/MM) simulations for organic and enzymatic reactions, Accounts of Chemical Research 43 (1) (2010) 142–151.
[46] X.L. Pan, F.C. Cui, W. Liu, J.Y. Liu, QM/MM study on the catalytic mechanism of heme-containing aliphatic aldoxime dehydratase, Journal of Physical Chemistry B 116 (19) (2012) 5689–5693.
[47] P.J. Silva, P.A. Fernandes, M.J. Ramos, A theoretical study of radical-only and combined radical/carbocationic mechanisms of arachidonic acid cyclooxygenation by prostaglandin H synthase, Theoretical Chemistry Accounts 110 (5) (2003) 345–351.
[48] D. Bakowies, W. Thiel, Hybrid models for combined quantum mechanical and molecular mechanical approaches, Journal of Physical Chemistry 100 (25) (1996) 10580–10594.
[49] I. Komaromi, L. Muszbek, Applications of the IMOMM (Integrated Molecular Orbital Molecular Mechanics) method for biopolymers, in: E. Buzaneva, P. Scharff (Eds.), Frontiers of Multifunctional Nanosystems, Kluwer Academic Publishers, Dordrecht, 2002, pp. 17–28.
[50] T. Vreven, K.S. Byun, I. Komaromi, S. Dapprich, J.A. Montgomery, K. Morokuma, M.J. Frisch, Combining quantum mechanics methods with molecular mechanics methods in ONIOM, Journal of Chemical Theory and Computation 2 (3) (2006) 815–826.
[51] K. Gupta, B.S. Selinsky, P.J. Loll, 2.0 angstroms structure of prostaglandin H2 synthase-1 reconstituted with a manganese porphyrin cofactor, Acta Crystallographica. Section D: Biological Crystallography 62 (2) (2006) 151–156.
[52] D.E. Krieger, YASARA, www.yasara.org, 2009.
[53] G.M. Morris, R. Huey, W. Lindstrom, M.F. Sanner, R.K. Belew, D.S. Goodsell, A.J. Olson, AutoDock4 and AutoDockTools4. Automated docking with selective receptor flexibility, Journal of Computational Chemistry 30 (16) (2009) 2785–2791.
[54] G.M. Morris, D.S. Goodsell, R.S. Halliday, R. Huey, W.E. Hart, R.K. Belew, A.J. Olson, Automated docking using a Lamarckian genetic algorithm and an empirical binding free energy function, Journal of Computational Chemistry 19 (14) (1998) 1639–1662.
[55] W.D. Cornell, P. Cieplak, C.I. Bayly, I.R. Gould, K.M. Merz, D.M. Ferguson, D.C. Spellmeyer, T. Fox, J.W. Caldwell, P.A. Kollman, A 2nd generation force-field for the simulation of proteins, nucleic-acids, and organic-molecules, Journal of the American Chemical Society 117 (19) (1995) 5179–5197.
[56] S. Dapprich, I. Komaromi, K.S. Byun, K. Morokuma, M.J. Frisch, A new ONIOM implementation in Gaussian98. Part I. The calculation of energies, gradients, vibrational frequencies and electric field derivatives, Journal of Molecular Structure: Theochem 462 (1999) 1–21.

[57] S. Grimme, Semiempirical GGA-type density functional constructed with a long-range dispersion correction, Journal of Computational Chemistry 27 (15) (2006) 1787–1799.
[58] L.A. Burns, A. Vazquez-Mayagoitia, B.G. Sumpter, C.D. Sherrill, Density-functional approaches to noncovalent interactions: a comparison of dispersion corrections (DFT-D), exchange-hole dipole moment (XDM) theory, and specialized functionals, Journal of Chemical Physics 134 (8) (2011).
[59] M.J. Frisch, G.W. Trucks, H.B. Schlegel, G.E. Scuseria, M.A. Robb, J.R. Cheeseman, J.A. Montgomery, T. Vreven, K.N. Kudin, J.C. Burant, J.M. Millam, S.S. Iyengar, J. Tomasi, V. Barone, B. Mennucci, M. Cossi, G. Scalmani, N. Rega, G.A. Petersson, H. Nakatsuji, M. Hada, M. Ehara, K. Toyota, R. Fukuda, J. Hasegawa, M. Ishida, T. Nakajima, Y. Honda, O. Kitao, H. Nakai, M. Klene, X. Li, J.E. Knox, H.P. Hratchian, J.B. Cross, V. Bakken, C. Adamo, J. Jaramillo, R. Gomperts, R.E. Stratmann, O. Yazyev, A.J. Austin, R. Cammi, C. Pomelli, J.W. Ochterski, P.Y. Ayala, K. Morokuma, G.A. Voth, P. Salvador, J.J. Dannenberg, V.G. Zakrzewski, S. Dapprich, A.D. Daniels, M.C. Strain, O. Farkas, D.K. Malick, A.D. Rabuck, K. Raghavachari, J.B. Foresman, J.V. Ortiz, Q. Cui, A.G. Baboul, S. Clifford, J. Cioslowski, B.B. Stefanov, G. Liu, A. Liashenko, P. Piskorz, I. Komaromi, R.L. Martin, D.J. Fox, T. Keith, M.A. Al-Laham, C.Y. Peng, A. Nanayakkara, M. Challacombe, P.M.W. Gill, B. Johnson, W. Chen, M.W. Wong, C. Gonzalez, J.A. Pople, Gaussian 03, in: Revision C. 02, Gaussian, Inc., Wallingford CT, 2004.
[60] M.J. Frisch, G.W. Trucks, H.B. Schlegel, G.E. Scuseria, M.A. Robb, J.R. Cheeseman, G. Scalmani, V. Barone, B. Mennucci, G.A. Petersson, H. Nakatsuji, M. Caricato, X. Li, H.P. Hratchian, A.F. Izmaylov, J. Bloino, G. Zheng, J.L. Sonnenberg, M. Hada, M. Ehara, K. Toyota, R. Fukuda, J. Hasegawa, M. Ishida, T. Nakajima, Y. Honda, O. Kitao, H. Nakai, T. Vreven, J.A. Montgomery, J.E. Peralta, F. Ogliaro, M. Bearpark, J.J. Heyd, E. Brothers, K.N. Kudin, V.N. Staroverov, R. Kobayashi, J. Normand, K. Raghavachari, A. Rendell, J.C. Burant, S.S. Iyengar, J. Tomasi, M. Cossi, N. Rega, N.J. Millam, M. Klene, J.E. Knox, J.B. Cross, V. Bakken, C. Adamo, J. Jaramillo, R. Gomperts, R.E. Stratmann, O. Yazyev, A.J. Austin, R. Cammi, C. Pomelli, J.W. Ochterski, R.L. Martin, K. Morokuma, V.G. Zakrzewski, G.A. Voth, P. Salvador, J.J. Dannenberg, S. Dapprich, A.D. Daniels, Ö. Farkas, J.B. Foresman, J.V. Ortiz, J. Cioslowski, D.J. Fox, Gaussian 09, in: Revision A.1, Gaussian, Inc., Wallingford CT, 2009.
[61] U. Varetto, Molekel 5. 4, Swiss National Supercomputing Centre, Manno, Switzerland, 2009.
[62] E.F. Pettersen, T.D. Goddard, C.C. Huang, G.S. Couch, D.M. Greenblatt, E.C. Meng, T.E. Ferrin, UCSF Chimera – a visualization system for exploratory research and analysis, Journal of Computational Chemistry 25 (13) (2004) 1605–1612.
[63] W. Humphrey, A. Dalke, K. Schulten, VMD. – visual molecular dynamics, Journal of Molecular Graphics 14 (1996) 33–38.
[64] DPlot, http://www.dplot.com/index.htm
[65] P. Gouet, X. Robert, E. Courcelle, ESPript/ENDscript: extracting and rendering sequence and 3D information from atomic structures of proteins, Nucleic Acids Research 31 (13) (2003) 3320–3323.
[66] R.A. Laskowski, M.W. MacArthur, D.S. Moss, J.M. Thornton, PROCHECK: a program to check the stereochemical quality of protein structures, Journal of Applied Crystallography 26 (1993) 283–291.
[67] J.U. Bowie, R. Luthy, D. Eisenberg, A method to identify protein sequences that fold into a known three-dimensional structure, Science 253 (5016) (1991) 164–170.
[68] R. Luthy, J.U. Bowie, D. Eisenberg, Assessment of protein models with three-dimensional profiles, Nature 356 (6364) (1992) 83–85.
[69] I.N. Levine, Quantum Chemistry, Pearson Prentice Hall, Upper Saddle River, 2009.
[70] I. Komaromi, J.M.J. Tronchet, Quantum chemical reaction path and transition state for a model cope (and reverse cope) elimination, Journal of Physical Chemistry A 101 (19) (1997) 3554–3560.
[71] J.J. Zheng, Y. Zhao, D.G. Truhlar, Representative benchmark suites for barrier heights of diverse reaction types and assessment of electronic structure methods for thermochemical kinetics, Journal of Chemical Theory and Computation 3 (2) (2007) 569–582.
[72] D.L. DeWitt, E.A. el-Harith, S.A. Kraemer, M.J. Andrews, E.F. Yao, R.L. Armstrong, W.L. Smith, The aspirin and heme-binding sites of ovine and murine prostaglandin endoperoxide synthases, Journal of Biological Chemistry 265 (9) (1990) 5192–5198.
[73] D.M. Friedrich, Z. Wang, A.G. Joly, K.A. Peterson, P.R. Callis, Ground-state proton-transfer tautomer of the salicylate anion, Journal of Physical Chemistry A 103 (48) (1999) 9644–9653.